Compact Wideband and Low-Profile Antenna Mountable on Large Metallic Surfaces

Zhang, Shuai; Pedersen, Gert F.

Published in:
I E E E Transactions on Antennas and Propagation

DOI (link to publication from Publisher):
10.1109/TAP.2016.2627008

Publication date:
2017

Document Version
Accepted author manuscript, peer reviewed version

Compact Wideband and Low-Profile Antenna Mountable on Large Metallic Surfaces

Shuai Zhang, and Gert Frølund Pedersen, *Senior Member, IEEE*

***Abstract*—This paper proposes a compact wideband and low-profile antenna mountable on large metallic surfaces. Six rows of coupled microstrip resonators with different lengths are printed on a Teflon block. The lengths of the microstrip resonators in different rows are gradually reduced along the end-fire direction. The first four rows of resonators provide four resonances at different frequencies for bandwidth enhancement. The last two rows of resonators are used as two directors to suppress sidelobe levels at high frequencies. A trapezoidal launcher is applied to serve as a reflector and provide one resonance at the lowest frequency. A trapezoid-shaped capacitive-feed (C-fed) strip is utilized and also printed on the Teflon block to globally optimize the wideband impedance matching. The proposed antenna covers a relative bandwidth of 109% for VSWR<2 with a height of 0.044 λ_L and a volume of only 0.03 λ_L^3 (λ_L being the free-space wavelength at the lowest operating frequency). Within the operating band, the realized gain is better than 6.5 dBi and the radiation efficiency is higher than 95%.**

***Index Terms*—Low-profile, wideband antenna, end-fire radiation, vertical polarization, large metallic surface, coupled microstrip resonator.**

I. Introduction

WIDEBAND antennas with end-fire radiation and vertical polarization have been widely used in the applications of aircrafts, missiles, wind turbine blade deflection sensing systems [1] and unmanned aerial vehicles. These applications require the wideband antenna have extremely low profile and small volume due to aerodynamics. Furthermore, the antennas should be able to be mountable on the large metallic platforms in these applications. However, it is very challenging to design the wideband antennas satisfying all the above mentioned requirements.

In the recent years, different techniques have been utilized to propose wideband flush-mounted antennas with low profile and end-fire radiation [2]-[16]. Microstrip Yagi array antennas have been first introduced in [2] and further developed in [3]-[6] with the advantages of end-fire radiation, low profile and low cost. However, the relative bandwidth of the antennas in [3]-[6] are smaller than 20%. In [7], a top-hat monopole Yagi antenna has been designed with the bandwidth of 20.5% and the height of 0.032 λ_L. In [8], by utilizing a series fed, the bandwidth of a microstrip Yagi magnetic dipole array has been extended to 28.6% while still keeping the low profile. H-plane horn antennas are another promising candidates [9]-[13]. Thin and compact SIW horn antennas have been designed in [9] and [10] with the thickness of larger than 0.08 λ_L and the bandwidth of narrower than 17%. Two rows of symmetrical coupled transition lines with and without gratings have been utilized in [10] and [9], respectively. The rows of the symmetrical transition lines with or without gratings are suggested to be no more than three. However, the antennas in [9] and [10] cannot be mounted on large metallic surfaces. A meshed horn antenna has been introduced in [11] with the height of 0.075 λ_L and bandwidth of 55%. The bandwidth in [11] has been enlarged by using a T-shaped feeding which provides another resonance. Thin ridged H-plane SIW horns have been investigated in [12] and [13] to further enhance the bandwidth. In [13], the antenna bandwidth is 93% with the thickness of 0.07 λ_L. However, the antenna feeding geometry in [13] is complicated and the impedance bandwidth is only matched to VSWR < 2.5 instead of 2. Surface wave antennas have been studied in [14]-[16]. In [16], a surface wave antenna with a very low profile of 0.061 λ_L has been reported. The bandwidth of the antenna is 98.8% for VSWR < 2 with the gain of better than 4 dBi and the simulated radiation efficiency of over 86%. However, the bandwidth of the antenna in [16] highly depends on the length of the high-permittivity dielectric slab, which limits the reduction of the antenna volume.

The concept of coupled microstrip resonators can be used to improve the impedance bandwidth of an antenna, e.g., in [17]. However, the bandwidth with coupled microstrip resonators in the previous publications is still too narrow for the applications of this paper. For example, the fractional bandwidth in [17] is only 10% with the thickness of 0.032 λ_L and broadside radiation instead of endfire radiation. Furthermore, in the applications of this paper, the antenna should not only own large impedance bandwidth, but also need to satisfy the requirements of very low profile, small volume, high radiation efficiency, easy of fabrication, endfire radiation and mounting on large metallic platforms simultaneously. The concept of coupled microstrip resonators has not been used to design antennas (satisfying all of these requirements) for the research areas introduced in this paper before.

In this paper, a compact wideband and low-profile antenna is designed, which is mountable on large metallic surfaces. Six rows of coupled microstrip resonators, printed on a Teflon block, are employed with their lengths in different rows decreasing gradually along the end-fire direction. The first four rows of resonators provide four resonances at different frequencies to broaden the impedance bandwidth, while the last

This work was supported by the InnovationsFonden project of "Intelligent rotor for wind energy cost reduction".

Shuai Zhang, and Gert Frølund Pedersen are with the Antennas, Propagation and Radio Networking section at the Department of Electronic Systems, Aalborg University, Denmark (email: sz@es.aau.dk).

two rows of resonators are used as two directors to suppress the sidelobe levels at high frequencies. A trapezoidal launcher is used to excite the six rows of coupled microstrip resonators, work as a reflector and provide one resonance at the lowest frequency. A trapezoid-shaped C-fed strip is utilized for wideband impedance matching, which is also printed on the Teflon block for ease of fabrication. With the proposed method, the designed antenna can be fabricated in a simpler and lower-cost way than relevant reported works. The bandwidth of the proposed antenna is over 109% for VSWR<2 with the thickness of 0.044 λ_L. Within the operating band, the realized gain is higher than 6.5 dBi and the radiation efficiency is over 95%. The volume of the proposed antenna is 0.03 λ_L^3. The volume and the height of the designed antenna are nearly 50% smaller and 28% lower than the antenna in [16], respectively.

II. Antenna Configuration

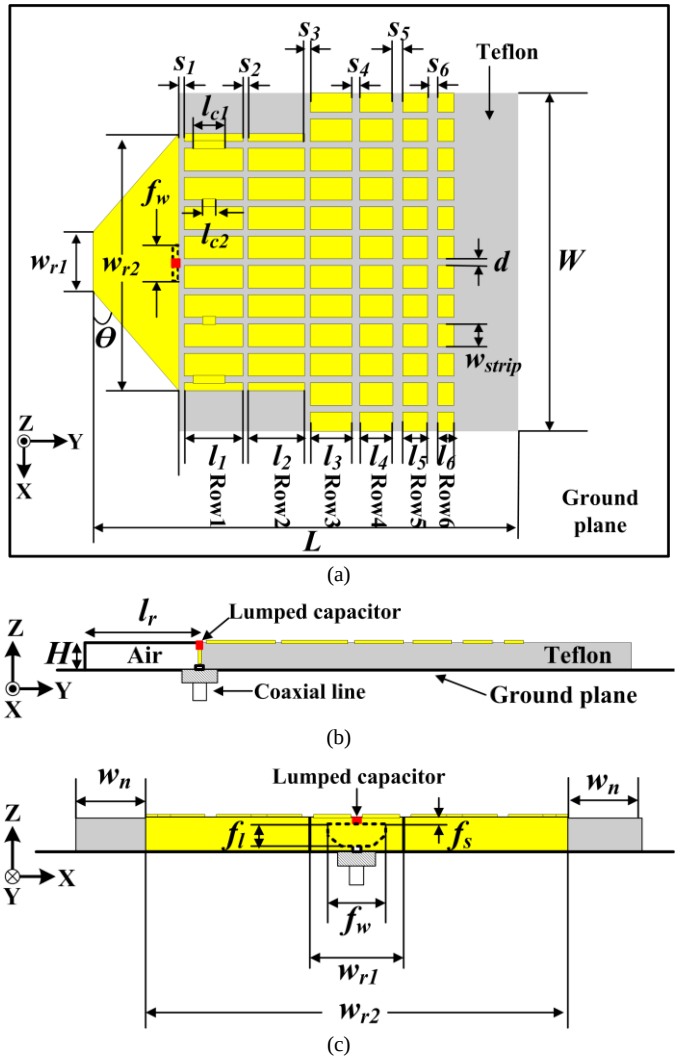

Fig. 1. Antenna geometry in: (a) xy plane, (b) yz plane, and (c) xz plane.

The geometry of the proposed antenna is illustrated in Fig.1. The antenna is placed on a large copper ground plane. The volume of the antenna is 75×95×4.5 mm^3. Six rows of coupled microstrip resonators are used and printed on a 4.5 mm-thick Teflon block. The permittivity and loss tangent of Teflon are 2.1 and 0.002, respectively. The lengths and widths of the microstrip resonators in the *i*th row are l_i (i=1, 2, 3, 4, 5, 6) and w_{strip}, respectively (see Fig. 1 (a)). The gaps between two neighboring microstrip resonators in y-axis direction and x-axis direction are s_j (j=1, 2, 3, 4, 5, 6) and d, respectively (see Fig. 1 (a)). A trapezoidal copper waveguide is placed next to and behind the Teflon block as a launcher (see Fig. 1 (b) and (c)). Four copper strips (with lengths of l_{c1} *and* l_{c2} in Fig. 1 (a)) are introduced to connect some of the microstrip resonators in the row next to the launcher together. These four connecting copper strips can help further suppress the sidelobe levels in xy plane at high frequencies. The C-fed method has been widely used for wideband impedance matching in mobile terminal antenna designs [18]-[20]. In this paper, a trapezoid-shaped C-fed strip is employed for the optimization of the wideband impedance, which is also printed on the Teflon block. In practice, the microstrip resonators and the C-fed strip can be painted on a Teflon block directly, which is a very popular technique for the manufacture of conformal mobile terminal antennas. Therefore, the proposed antenna is relatively easier to fabricate than the designs in [13] and [16]. In addition, a 0.4 pF lumped capacitor is inserted between the C-fed strip and the trapezoidal launcher to simplify the manual fabrication of the prototype. The detailed dimensions of the designed antenna are listed in Table I.

TABLE I
Detailed Dimensions of the Designed Antenna

Parameter	Value (mm)	Parameter	Value (mm)
l_1	13	W	75
l_2	12.5	L	95
l_3	9.2	H	4.5
l_4	7.3	l_r	19
l_5	5.5	w_{r1}	13.4
l_6	3.6	w_{r2}	57
s_1	0.4	θ	41.07°
s_2	0.5	l_{c1}	7
s_3	0.5	l_{c2}	2
s_4	1	w_n	9
s_5	1	f_l	3.5
s_6	1	f_s	0.5
w_{strip}	5	f_w	9
d	1.5		

III. Underlying Operating Mechanisms

The compact wideband and low-profile antenna is designed to be mounted on a large metallic platform. Therefore, the performance of the antenna will be analyzed on an infinitely-large ground plane. In addition, all the simulations in this paper are carried out with the software of CST Microwave Studio 2015 and 2016. Optimizations are carried out by sweeping each parameter to find an approximate value in CST first, and then apply interpolated quasi newton method in CST to search the optimal values of all the parameters automatically.

The simulated VSWR of the designed antenna on an infinitely-large ground plane is shown in Fig. 2. It is seen that the antenna covers the wideband of 2.95-10 GHz for VSWR< 2. Normalized radiation patterns in *xy* plane and *yz* plane are

given in Fig. 3 at 3.5 GHz, 5.5 GHz, 7.5 GHz and 9.5 GHz. Within the operating band, the main beam of the antenna is always pointing at the +y axis (see Fig. 1) direction (end-fire radiation). In the following, the studies will be focused on investigating the bandwidth and the sidelobe levels of the proposed antenna.

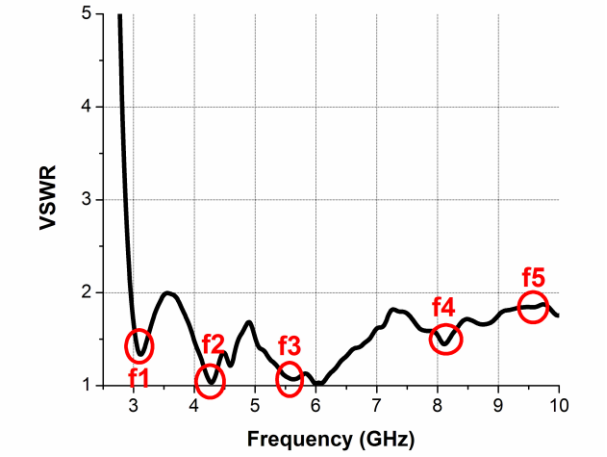

Fig. 2. VSWR of the proposed antenna on an infinite ground plane.

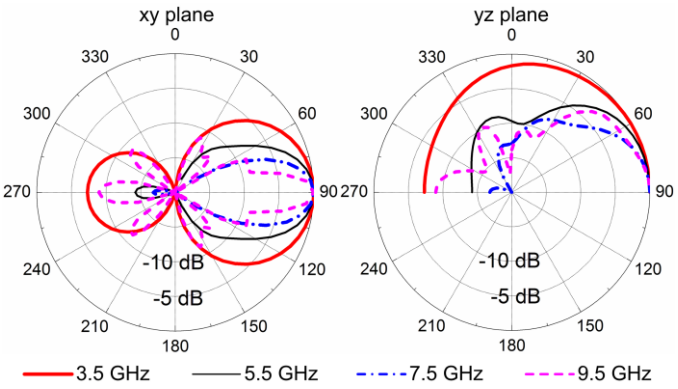

Fig. 3. Normalized radiation patterns of the proposed antenna on an infinite ground plane in xy plane and yz plane at different frequencies.

A. Trapezoidal Launcher

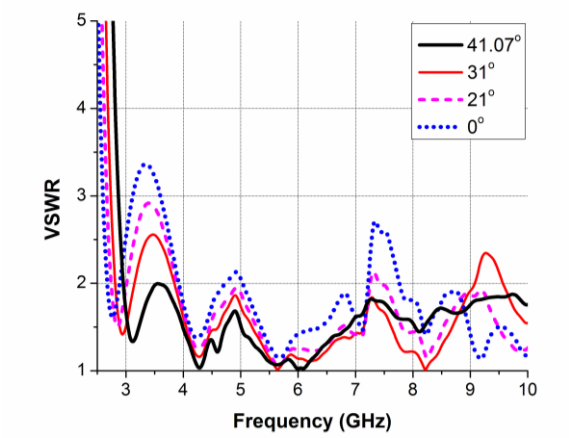

Fig. 4. VSWR for the trapezoidal launcher with different angle θ.

A trapezoidal launcher is utilized to excite the six rows of coupled microstrip resonators and provide one resonance at the lowest frequency of around 3.1 GHz (see f1 in Fig. 2). The launcher also works as a reflector, where the sidelobe levels can be suppressed by adjusting the shape of the reflecting wall. Please note that the launcher can also be realized in some other ways instead of a waveguide type as long as it is able to excite the resonators.

The VSWR is shown in Fig. 4 for the trapezoidal launcher with different angle θ (see Fig. 1) while keeping w_{r1}, w_{r2} and l_r unchanged. When the angle θ decreases from 41.07° to 0°, the cavity of the launcher becomes bigger and the resonance at around 3 GHz also moves to lower frequencies. θ = 0° means the trapezoidal launcher has been modified into a rectangular launcher. It is also noticed that the VSWR higher than 4 GHz can also be slightly improved by selecting the right angle, i.e., 41.07°.

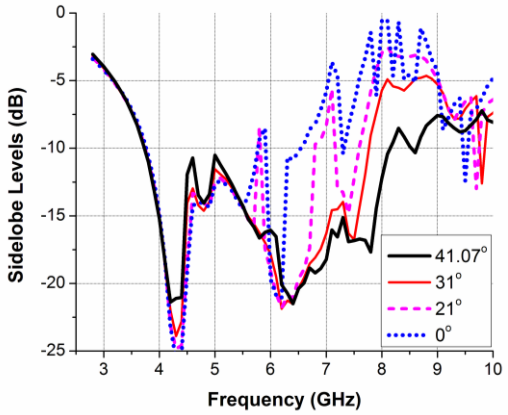

Fig. 5. Sidelobe levels in xy plane for the trapezoidal launcher with different angle θ.

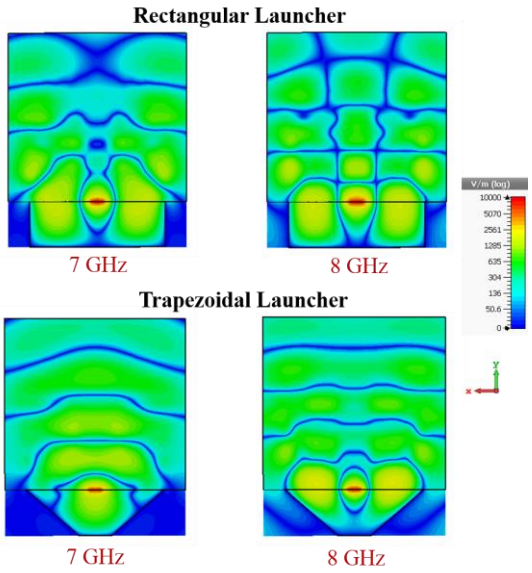

Fig. 6. Simulated electric field distributions on the ground plane with a rectangular launcher and with a trapezoidal launcher.

Adjusting the angle θ changes the phase and amplitude of the electric field along the aperture width of the launcher, which mainly affects the radiation patterns in *xy* plane. The sidelobe levels in *xy* plane with different angle θ are shown in Fig. 5.The side lobes can be much more efficiently suppressed with the angle increasing from 0° to 41.07° over the wide bandwidth. Electric field distributions on the ground plane (*xy* plane) are given in Fig. 6. It is clearly observed that the radiated

electromagnetic waves (from the end of the antenna) with a trapezoidal launcher are more similar to quasi-plane waves than with a rectangular launcher. This can also explain the relatively lower sidelobe levels in *xy* plane with a trapezoidal launcher. In addition, it is also noticed that the inside of the trapezoidal launcher is filled with the air instead of any dielectric material (see Fig. 1). There are two reasons: 1. It is easier to achieve wideband impedance matching with the air filled for our proposed low-profile antenna than with a dielectric material filled; 2. With the air filled, the trapezoid-shaped feed strip can be painted on a Teflon block directly (for the ease for fabrication), while the metal trapezoidal copper launcher can be milled into one piece mechanically.

Compared with the super-elliptical launcher in [10] and the modified parabolic launcher in [16], the trapezoidal one used in this paper occupies a much smaller volume and easier for fabrication. The purpose of using a super-elliptical or the modified parabolic is to realize quasi-plane waves at the aperture of a launcher. Similar to the modified parabolic reflector in [16], the trapezoidal-shaped waveguide in this paper also works as a reflector instead of a planar horn. Since the C-fed strip (see Fig.1) will be painted on a Teflon block to facilitate fabrication, the reflector length of l_r (see Fig. 1) has to be the same to the distance between the C-fed strip and the bottom of the reflecting wall, where the distance is larger than a quarter but less than a half guided wavelength (at the center frequency) [16]. The l_r in this paper is much shorter than those in [10] and in [16]. Shorter l_r gives smaller launcher volume, but it is less effective to realize quasi-plane waves (and low sidelobe levels in *xy* plane) at high frequencies where some higher order TE modes are supported by the reflector aperture. However, in the following we will show that the sidelobe levels at high frequencies can be further suppressed with the last two rows of coupled microstrip resonators and four copper strips (with lengths of l_{c1} and l_{c2} in Fig. 1 (a)). In this way, the proposed antenna can realize a compact volume and sidelobe levels lower than -7.2 dB at higher frequencies at the same time.

B. Coupled Microstrip Resonators

1) Different Rows of Coupled Microstrip Resonators

Coupled microstrip resonators are the main crucial factor for achieving large impedance bandwidth while maintaining the low profile of the designed antenna. The fundamental theory about coupled parallel microstrip lines or resonators can be found in [21]-[23]. In this paper, there are six rows of coupled microstrip resonators with different lengths of l_i (i=1, 2, 3, 4, 5, 6) and the gaps of s_j (j=1, 2, 3, 4, 5, 6) (see Fig. 1). In general, the operating frequencies of the resonances produced by the microstrip resonators are mainly determined by the lengths of l_i. The gaps of s_j are used to efficiently excite the resonances provided by the microstrip resonators. In this design, the first four rows of resonators (with lengths of l_i (i=1, 2, 3, 4) and the gaps of s_j (j=1, 2, 3, 4)) are utilized to provide four resonances at around 4.2 GHz, 5.6 GHz, 8.3GHz and 9.5 GHz (see f2, f3, f4, f5 in Fig. 2) to enlarge the bandwidth. Since four rows of resonators are already sufficient to cover the wide bandwidth, the last two rows of resonators (with lengths of l_i (i=5, 6) and the gaps of s_j (j=5, 6)) are designed as two directors to suppress the sidelobe levels at high frequencies. Please note in Fig. 2 there are also some other resonances besides f1 to f5. These additional resonances are a kind of parasitic slot modes formed by the neighboring coupled resonators within each row. In Section III B 3), we will show that this kind of modes slightly changes the antenna performance but will not affect the practical applications.

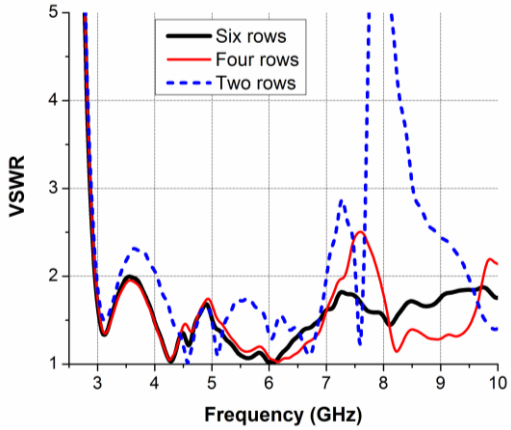

Fig. 7. VSWR of the proposed antenna with different rows of microstrip resonators.

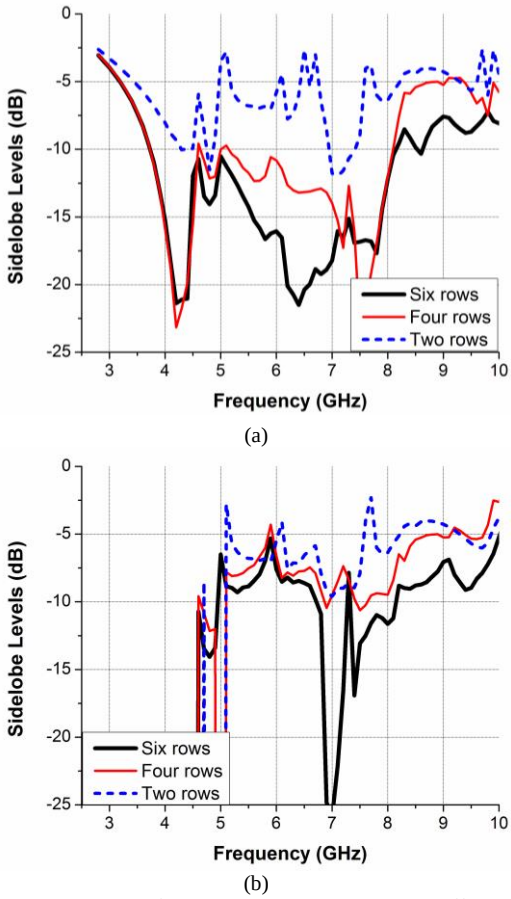

Fig. 8. Sidelobe levels of the proposed antenna with different rows of microstrip resonators: (a) in xy plane, and (b) in yz plane.

The VSWR of the proposed antenna with different rows of microstrip resonators is provided in Fig. 7. It is observed that:

with the rows increasing from two to four, the bandwidth is mainly improved at the frequencies of 7-10 GHz. There is some detuning at around 7.5 GHz and 10 GHz, since the resonances introduced by the third and fourth rows of resonators have shifted to higher frequencies. However, the detuning can be eliminated by adjusting the lengths and gaps of the first four rows of resonators. The VSWR improvement with the rows increasing from four to six is less than that from two to four. Furthermore, the sidelobe levels of the proposed antenna with different rows of microstrip resonators are shown in Fig. 8. Increasing rows from two to four mainly suppress the sidelobe levels in *xy* plane at low frequencies. As we expected, when the rows change from four to six, the sidelobe levels in both *xy* plane and *yz* plane are improved efficiently at high frequencies. The front-to-back ratio (FTBR) and 3 dB beam width of the proposed antenna are also provided and listed in Table II. In general, the FTBR is better than the sidelobe level suppression. The 3 dB beam widths in *xy* plane and *yz* plane are 14.3-72.6 degree and 31.5-127.3 degree, respectively. Please note when the rows are more than six, the energy coupled to the seventh row is already very weak, so the improvement on the bandwidth and the sidelobe levels is nearly negligible.

TABLE II
FRONT-TO-BACK RATIO AND 3DB BEAM WIDTH

f (GHz)	3	4	5	6
front-to-back ratio (dB)	4.0	15.2	10.5	17.4
3 dB beam width in xy plane(degree)	72.6	58.4	52.7	40.4
3 dB beam width in yz plane(degree)	127.3	96.5	53.1	38.6
f (GHz)	7	8	9	10
front-to-back ratio (dB)	25.9	17.9	11.2	9.6
3 dB beam width in xy plane(degree)	32.4	20.7	14.3	24.0
3 dB beam width in yz plane(degree)	33.3	31.5	45.9	39.2

2) Study of the Lengths l_i and the Gaps s_j of Coupled Microstrip Resonators

Utilizing the methods in [9] or [17], it is possible to calculate and predict the lengths (l_i) and the gaps (s_j) of different rows of coupled microstrip resonators. However, the calculations will be very complex, if considering the number of the resonator rows as well as the unequal lengths and gaps of different rows. Furthermore, the cutting slots along *y*-axis direction (with the width of *d*, see Fig. 1) decrease the capacitor of each row, which will affect the accuracy of calculations. Therefore, in this paper, the lengths of l_i and the gaps of s_j are determined by full-wave simulations with the software of CST. Since the first four rows of coupled resonators are responsible for enhancing impedance bandwidth, detailed parametric studies of the lengths (l_1, l_2, l_3, l_4) and the gaps (s_1, s_2, s_3, s_4) are carried out to facilitate the simulations.

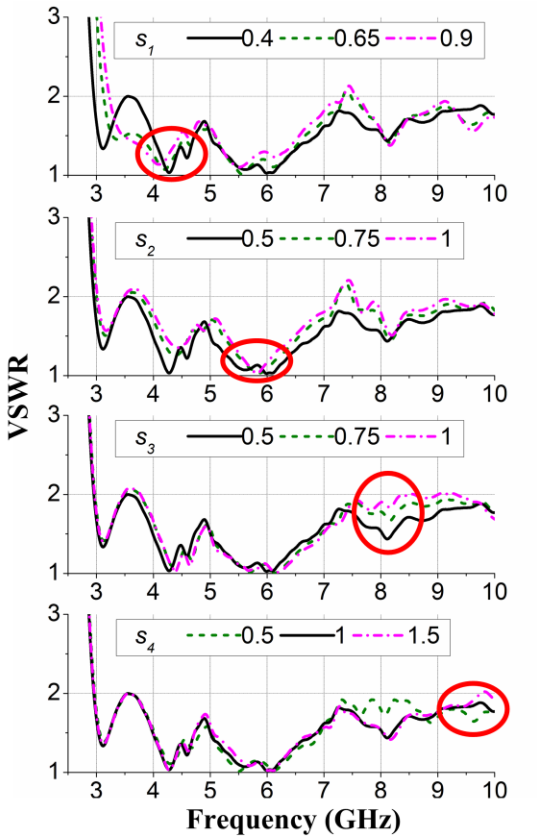

Fig. 9. VSWR with different values of gaps of s_j (j = 1, 2, 3, 4).

The resonances of f2, f3, f4 and f5 (see Fig. 2) are generated by the row1, row2, row3 and row4 (see Fig.1 (a)) of the coupled microstrip resonators, respectively. By increasing the number of rows from 1 to 4, every time a new row is added (with the parameters of the whole antenna slightly adjusted), one more resonance can be obtained. If only resonator row1 is available, the antenna will have two resonances of f1 (provided by the trapezoidal launcher) and f2. When we introduce the resonator row2, the mutual coupling between row1 and row2 will enlarge the capacitor of row1 and decrease the capacitor of row2 to store charges [9][21]. Therefore, f2 and f3 will move to relatively lower and relatively higher frequencies, respectively. Similarly, adding row3 into the antenna will make f3 and f4 move to relatively lower and relatively higher frequencies, respectively. The same phenomenon will also happen when we place row4 into the antenna. In this way, four resonances of f2, f3, f4 and f5 are provided by the first four rows of resonators. VSWR with different values of gaps of s_j (j= 1, 2, 3, 4) is given in Fig. 9, where the solid blade curve is plotted with the parameter values in Table I. These gaps adjust the mutual coupling between the neighboring rows. In Fig. 9, the gaps of s_1, s_2, s_3, and s_4 can be used to tune the impedance matching of f2, f3, f4 and f5, respectively. Please note that s_1 is the gap formed by the trapezoidal reflector and the first row of resonators, so changing s_1 will also shift the operating frequency of f1. VSWR with different lengths of l_i (i = 1, 2, 3, 4) is shown in Fig. 10, where the solid blade curve is plotted with the parameter values in Table I. The microstrip resonators in different rows are tightly coupled. In Fig. 10, changing the

length of one row will shift the resonant frequencies of not only the row itself, but also the neighboring rows and the rows behind. Therefore, the locations of f2, f3, f4 and f5 can be adjusted by changing the lengths of l_1, l_2, l_3 and l_4. With the tendency illustrated in Fig. 10, it is possible to properly arrange the locations of f2, f3, f4 and f5 for bandwidth improvement.

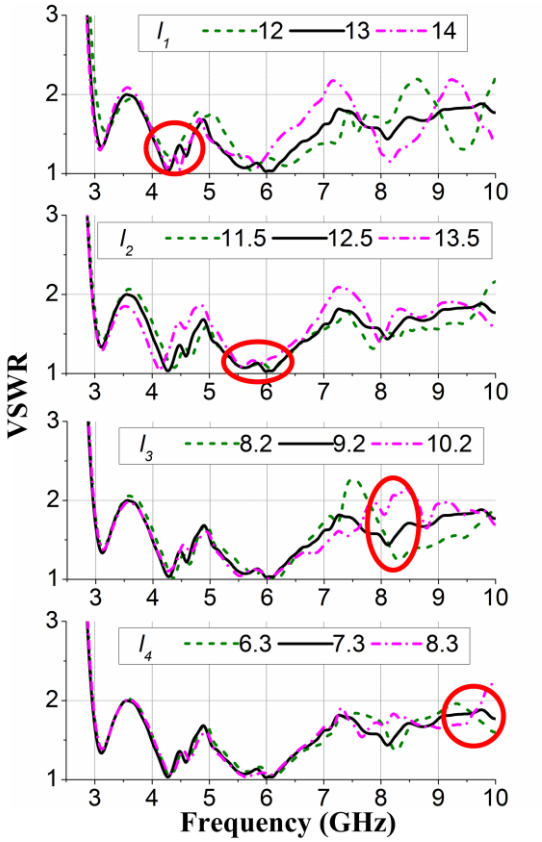

Fig. 10. VSWR with different lengths of l_i (i = 1, 2, 3, 4).

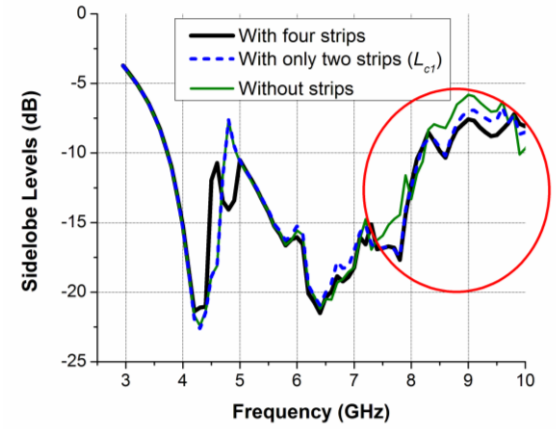

Fig. 11. Sidelobe levels in xy plane with and without copper strips (with lengths of l_{c1} *and* l_{c2}).

As mentioned above, the last two rows (see row5 and row6 in Fig. 1 (a)) of coupled resonators are designed as two directors to reduce the sidelobe levels at high frequencies. Since row5 is next to row4 the length l_5 will also affects the location of f5, while the VSWR from 2.95-10 GHz is not sensitive to the gaps of s_5, s_6 and the length of l_6. The sidelobe levels at high frequencies are more sensitive to the gaps of s_5 and s_6 than the lengths l_5 and l_6. Fig. 8 shows the effectiveness of two directors (as the rows increasing from four to six), where the sidelobe levels in both *xy* plane and *yz* plane are suppressed efficiently at high frequencies. In addition, four copper strips (with lengths of l_{c1} and l_{c2} in Fig. 1 (a)) are also utilized to connect some of the microstrip resonators in the row1 (see Fig. 1 (a)) together, which can help further suppress the sidelobe levels in *xy* plane at higher frequencies. As shown in Fig. 11, more sidelobe suppression in *xy* plane can be obtained from 7.5-9.8 GHz by four strips without distorting the radiation patterns in *yz* plane.

In the following, brief design guidelines are summarized to determine lengths of l_i (i=1, 2, 3, 4, 5, 6) and the gaps of s_j (j=1, 2, 3, 4, 5, 6): 1. Set the lengths (and the gaps) of different rows of resonators to be equal at the beginning; 2. Tune the gaps of the first four rows one by one to excite the introduced resonances efficiently; 3. Change the lengths of the first four rows to shift different resonances approximately to different frequencies for bandwidth enhancement; 4. Sweep the lengths and the gaps of the last two rows in CST to approximately set the values for sidelobe level reduction, 5. Utilize the optimization method of interpolated quasi newton in CST to optimize all the parameters. Please note that interpolated quasi newton is a local optimizer. Steps 1-4 are used to shorten the time for the optimizer to find out the optimal parameters.

3) Study of Parasitic Slot Modes of Microstrip Resonators

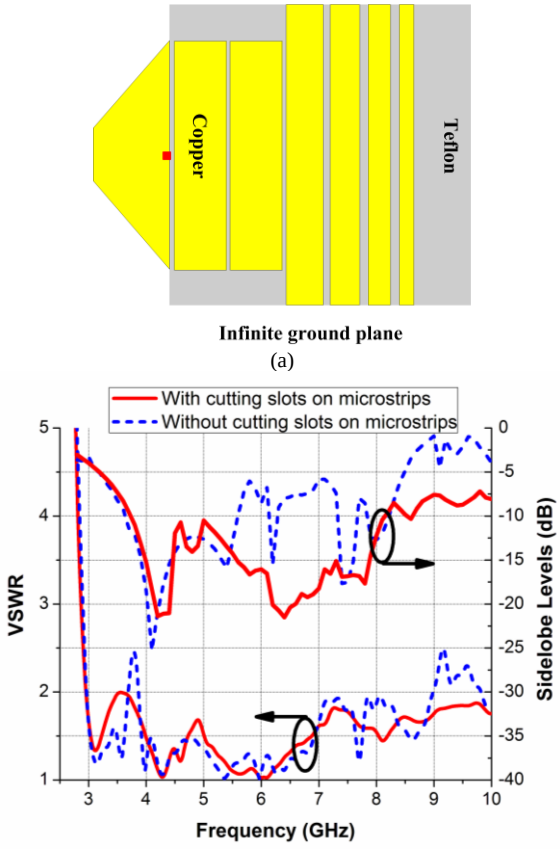

Fig. 12. (a) Antenna without cutting slots on microstrip lines, (b) comparison of VSWR and sidelobe levels in *xy* plane with or without cutting slots on microstrip lines.

To achieve large bandwidth and low antenna profile, some rows of coupled resonators have to be added. In order to make enough energy coupled to the last rows, the distances between the neighboring rows are small. Some parasitic slot modes in *x*-axis direction (see Fig. 1) can also be excited between the microstrips resonators in the neighboring rows (*x*-axis parasitic slot modes). These parasitic modes severely distort the end-fire radiation patterns and the impedance matching. Since the impedance of the proposed antenna is not sensitive to the widths of the microstrip resonators (w_{strip}). Some slots with the width of *d* (see Fig. 1) in *y*-axis direction has been cut on the microstrip lines. The widths (*d*) have to increase until the operating frequencies of the parasitic modes are out of the band of 2.95-10 GHz. This is quite different from the purpose of the rectangular grating transition introduced in [10]. The antenna without cutting slots on microstrip lines is illustrated in Fig. 12 (a). The sidelobe levels in *xy* plane and VSWR with or without cutting slots on microstrip lines are compared in Fig. 12 (b). Since the cutting slots on microstrips mainly affect the sidelobe levels in *xy* plane, the sidelobe levels in *yz* plane is not given in Fig. 12 (b). It is seen from Fig. 12 (b) that without cutting slots the sidelobe levels in *xy* plane and VSWR is much higher and noisier than the case with cutting slots, respectively.

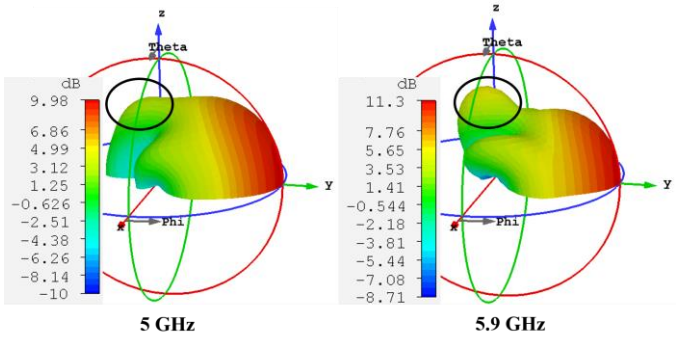

Fig. 13. Simulated radiation gain patterns at 5 GHz and 5.9 GHz.

The cutting slots along *y*-axis direction can eliminate *x*-axis parasitic slot modes within the operating band. In fact, these cutting slots will also introduce some other parasitic slot modes in *y*-axis direction (*y*-axis parasitic slot modes). In Fig. 2, some additional resonances (besides f1, f2, f3, f4 and f5) are from *y*-axis parasitic slot modes. However, compared with *x*-axis parasitic slot modes, *y*-axis parasitic slot modes are less efficiently excited and also fewer since the *y*-axis slots are 1.5-3 times as wide as the *x*-axis slots. Pease note Fig. 12 (a) is also the comparison between the cases only with *x*-axis parasitic slot modes and only with y-axis parasitic slot modes. The *y*-axis parasitic slot modes will also slightly distort the radiation patterns and lead to 1-2 dB realized gain variation, but it will not be an issue for practical applications. For example, the *yz*-plane sidelobe levels at around 5 GHz and 5.9 GHz in Fig. 8 (b) increase to -6.5 dB and -5.3 dB, respectively. It is due to the *y*-axis parasitic slot modes. The radiation gain patterns at 5 GHz and 5.9 GHz are shown in Fig.13. The increase of sidelobe levels is because a side lobe close to *z* axis becomes relatively stronger at 5 GHz and 5.9 GHz than the other frequencies. However, the radiation pattern around the endfire direction have little change and the side lobe is far away from the endfire direction, so the increase of sidelobe level due to *y*-axis parasitic slot modes has limited impacts on the practical applications, e.g., in [1]. In addition, further increasing the width *d* of the *y*-axis slot can weaken the *y*-axis parasitic slot modes, but it will reduce the impedance bandwidth to the smaller areas for metal resonators. It is also noticed that there is still a part of bare substrate without metal printing with the width of w_n, as shown in Fig.1. Paving more coupled resonators in the bare areas (from the first two rows) will improve the impedance bandwidth. However, it will also excite the *y*-axis parasitic slot mode at around 4.5 GHz very efficiently, where the bare areas are used to suppress it.

Therefore, there is a tradeoff between the impedance bandwidth and the suppression of (*x*-axis and *y*-axis) parasitic slot modes.

C. Capacitive Feed Structure

A trapezoid-shaped C-fed strip is implemented in this paper. The capacitive feed structure is mainly used to tune the wideband impedance matching so that all the above mentioned resonances of f1, f2, f3, f4 and f5 can operate simultaneously.

The C-fed strip is printed on the Teflon substrate (as shown in Fig. 1). Please note that in the experiment C-fed strip is realized by sticking a trapezoid-shaped copper tape on the substrate, while in practice it can be painted on the Teflon block directly. C-fed method is a well-known technique. The detailed study of C-fed method can be found in [18]. The shape of the strip (f_w and f_l in Fig. 1) and the distance (f_s) between the strip and launcher can change real and imaginary parts of the impedance over a wideband. Furthermore, in [24], different feed plate silhouettes have been studied to improve the bandwidth of a PIFA. Similar concept has also been used in this paper: the two bottom corners of the strip have been chamfered, and these chamfers are mainly used to tune the impedance matching at frequencies higher than 6 GHz.

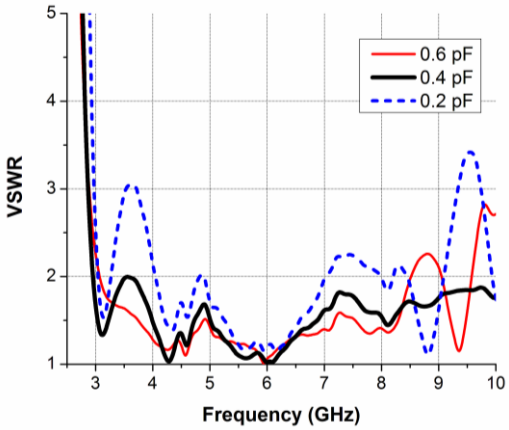

Fig. 14. VSWR of the proposed antenna with different capacitance for the lumped capacitor.

In order to obtain a good wideband impedance matching, a large capacitance is required between the strip and the launcher, which means the distance of f_s should be around 0.1 mm or 0.2 mm. In practice, since the feed strip and coupled microstrip resonators are painted on a Teflon block directly, it is easy to

control f_s to be 0.1 mm or 0.2 mm. In this paper, the prototype of the designed antenna is fabricated manually. In order to simplify the prototype fabrication, f_s is kept to 0.5 mm and a high-Q lumped capacitor is inserted between the top of feed strip and the launcher. The VSWR of the proposed antenna with different capacitance for the lumped capacitor is illustrated in Fig. 14. A good wideband impedance matching has been achieved with the capacitance of 0.4 pF.

IV. Simulated and Measured Antenna Performance on a Finite-Large Ground Plane

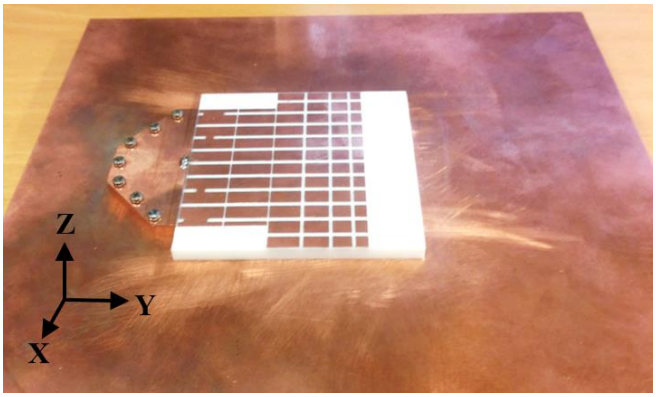

Fig. 15. Prototype of the compact wideband low-profile antenna on a 200 mm × 200 mm large ground plane.

The proposed wideband and low-profile antenna has been fabricated and placed on 200 mm ×200 mm large copper ground plane. The prototype is shown in Fig. 15, where the compactness of the antenna is clearly observed. In addition, some screws are used to stabilize the top copper plate of the launcher in the experiment. These screws will not affect antenna characteristics. In practical applications, the launcher waveguide will be milled mechanically into one piece, so no screws will be available on the top copper plate.

A. Impedance Bandwidth

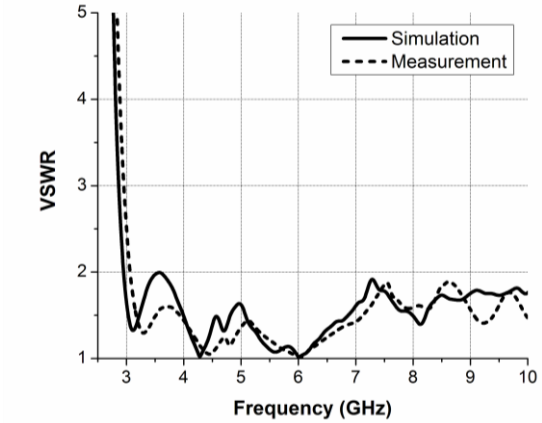

Fig. 16. Simulated and measured VSWR of the proposed compact wideband low-profile antenna on a 200 mm × 200 mm large ground plane.

The VSWR of the fabricated antenna on a 200 mm ×200 mm large ground plane has been measured with a network analyzer. The comparison between the simulated and measured VSWR can be obtained in Fig. 16. In general, the measured result agrees well with the simulation. The simulated bandwidth is 2.95-10 GHz, while the measured bandwidth is 3.06-10 GHz for VSWR <2. The measured lowest resonance has moved by around 100 MHz to the higher frequency than the simulated. The discrepancy is possibly due to the slightly smaller cavity dimensions of the trapezoidal launcher in the fabrication than those in the simulations.

Furthermore, the simulated VSWR with a 200 mm ×200 mm large ground plane in Fig. 16 is very similar to the simulated one with an infinitely large ground plane in Fig. 2. The impedance matching of the proposed antenna is not sensitive to the size of the ground plane.

B. Realized Gain and Radiation Patterns

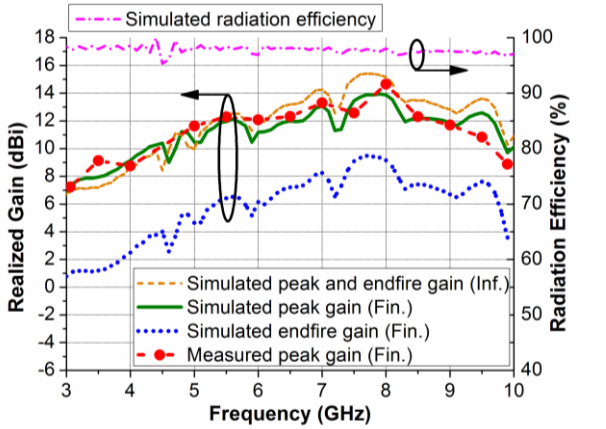

Fig. 17. Simulated and measured peak realized gain, simulated endfire gain and simulated radiation efficiency on a 200 mm × 200 mm large ground plane; simulated peak and endfire gain on an infinite ground plane.

The simulated and measured peak realized gain of the proposed antenna on a 200 mm ×200 mm large ground plane is compared and shown in Fig. 17. The measurement aligns very well with the simulation. The realized gain is from 6.5 dBi to 14.6 dBi with small antenna volume and thinness. Furthermore, the simulated endfire gain on an infinite and a 200 mm ×200 mm large ground plane is also added in Fig. 17. From the comparison, the two gain curves are almost parallel with each other and the difference between them is around 5 dBi. In addition, the simulated radiation efficiency is also plotted in Fig. 17. All the losses from copper and Teflon have been taken into account. The radiation efficiency is higher than 95% within the operating bandwidth.

Fig. 18 shows the sidelobe levels of the proposed antenna in *xy* plane and H plane on a 200 mm × 200 mm large ground plane, as well as in *xy* plane (or H plane) on an infinite ground plane. On an infinite ground plane, the *xy* plane is the antenna H plane. On a 200 mm ×200 mm large ground plane, the *xy* plane is not the H-plane any more since the main beam of the proposed antenna is tilted. However, it is interesting to see that the *xy*-plane sidelobe levels are almost the same regardless of the ground plane sizes. On a 200 mm × 200 mm large ground plane, the H-plane sidelobe levels are better than the xy-plane at most of the frequencies. In fact, since the main beam is tilted on a finite ground plane, the boundary conditions (in the opposite direction of the tilted main beam) for H-plane radiation patterns

TABLE III
PERFORMANCE COMPARISON OF COMPACT WIDEBAND AND LOW-PROFILE ANTENNAS

Reference	Bandwidth	Volume (λ_L^3)	Height (λ_L)	Gain (dBi)	η_{rad} (%)
[10]	16% for VSWR<2	0.278	0.089	6.5-8	-
[12]	76% for VSWR<2.5	1.490	0.152	5-10	>95%
[13]	93% for VSWR<2.5	0.135	0.070	1.5-14	-
[16]	98.8% for VSWR<2	0.059	0.061	4-12	>88%
This work	109% for VSWR<2	0.030	0.044	6.5-14.6	>95%

are not the same to the case on an infinite ground plane. In other words, the modification of H plane radiation patterns depends on how much the main beam is tilted, while the tilted angle of the main beam depends on the size of the ground plane. This is not related to antenna designs. The proposed antenna will be used on an electrically large metallic platforms (which can be considered as infinite ground plane), and communications will be built up around the endfire direction of the antenna in practical applications. Therefore, it is more meaningful to investigate the radiation patterns on *xy* plane instead of the H plane.

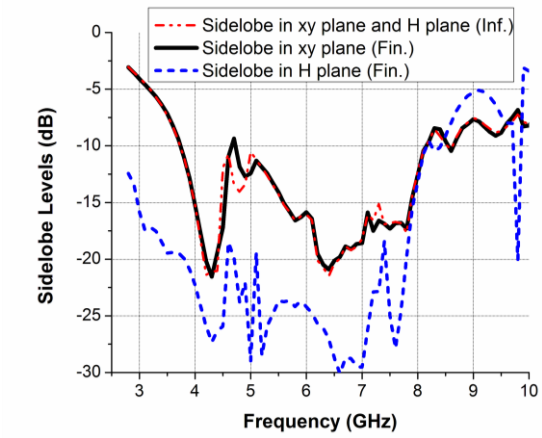

Fig. 18. Simulated sidelobe levels in *xy* plane and H plane on a 200 mm × 200 mm large ground plane, and simulated sidelobe levels in *xy* plane (or H plane) on an infinite ground plane.

Fig. 19 shows the normalized simulated and measured radiation patterns on a 200 mm ×200 mm large ground plane at 3.5 GHz, 5.5 GHz, 7.5 GHz, and 9.5 GHz. The radiation patterns are compared on both *yz* plane and *xy* plane. Since the cross-polarization radiation patterns are at least 10 dB lower in *xy* plane and at least 20 dB lower in *yz* plane than the co-polarization, only the co-polarization are plotted in Fig. 19. The discrepancy between the simulation and measurement is very small. Furthermore, the simulated normalized radiation patterns on an infinite ground plane are also added in Fig. 19 for comparisons. It is observed that the simulated normalized radiation patterns on *xy* plane are nearly the same regardless of the ground plane sizes. Please note that: in *xy* plane, the radiation gain patterns on a 200 mm ×200 mm large ground plane are around 5 dBi lower than those on an infinite ground plane. In addition, the antenna performance is not sensitive to the size of the ground plane. If the ground plane is wider than 200 mm (in x-axis direction), the radiation patterns in Fig. 19 are almost the same. If the ground plane is longer than 200 mm (in y-axis direction), the radiation beam in *yz* plane will gradually point towards the y-axis direction (end-fire direction).

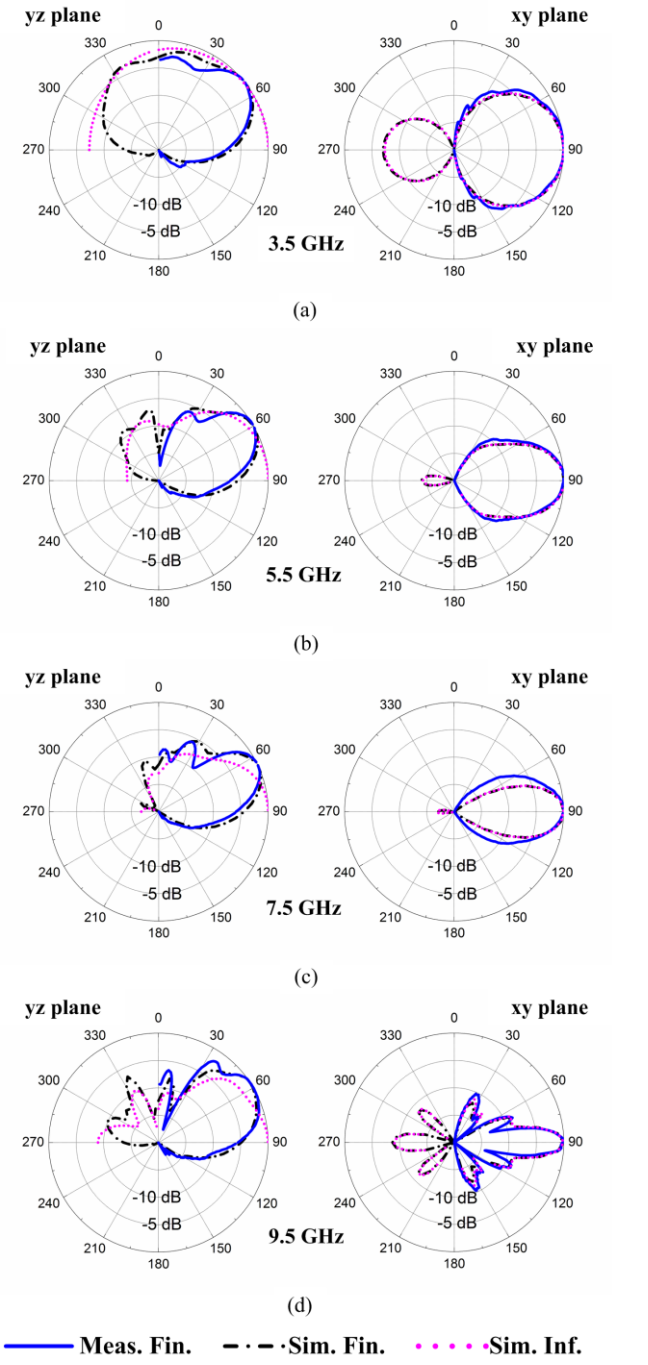

Fig. 19. Simulated and measured normalized radiation patterns in yz plane and xy plane at: (a) 3.5 GHz, (b) 5.5 GHz, (c) 7.5 GHz, and (d) 9.5 GHz.

C. Performance Comparison

A comparison between the proposed antenna and the previous work is listed in Table III. It is clearly seen that the proposed antenna has the best overall performance by considering bandwidth, volume, height, realized gain and radiation efficiency. Compared with the work in [16], the volume and the height of the designed antenna are nearly 50% smaller and 28% lower, respectively.

In addition, the works in [10] and [12] are designed for free space instead of large metallic surfaces. If we assume the antennas in [10] and [12] can be utilized on large metallic platforms, ideally the volume and the height of the antennas can be reduced by half of the current values. And we assume the bandwidth of antennas is kept the same (this is difficult to realize in practice). We can find that the volumes and heights of the antennas in [10] and [12] with large ground planes are still bigger and thicker than those of the proposed antenna. Furthermore, the bandwidth in [10] and [12] is narrower than the designed antenna as well. Furthermore, in [16] the antenna performance is evaluated on a small ground plane. If we reduce the ground plane size of our designed antenna into 75 mm × 160 mm (which is similar to electrical size in [16]), only the gain in Table III will change from 6.5-14.6 dBi into 6.5-13 dBi while keeping the other figure of merits in Table III the same.

V. Conclusions

A compact wideband and low-profile antenna has been proposed in this paper, which is mountable on large metallic surfaces. By utilizing six rows of coupled microstrip resonators, a trapezoidal launcher and a trapezoid-shaped C-fed strip, the proposed antenna has covered the relative bandwidth of 109% for VSWR<2 with the height of 0.044 λ_L. Within the operating band, good realized gain and radiation efficiency has been achieved. The volume of the proposed antenna is 0.03 λ_L^3 which is much smaller than previous reported in the literature.

Acknowledgment

The authors would like to thank Peter Boie Jensen, Jesper Dejgaard Pedersen and Ben Krøyer at Aalborg University for their help on the prototype fabrications.

References

[1] S. Zhang, T. L. Jensen, K. Olesen, O. Franek, P. C. F. Eggers, C. Byskov and G. F. Pendersen, "UWB wind turbine blade deflection sensing for wind energy cost reduction," *Sensors*, vol. 15, no. 8, pp. 19768-19782, 2015.

[2] J. Huang, "Planar microstrip Yagi array antenna," in *IEEE Antennas Propagat. Soc./Ursi Symposium Dig.*, June 1989, pp. 894-897.

[3] J. Huang and A. C. Densmore, "Microstrip Yagi array antenna for mobile satellite vehicle application," *IEEE Trans. Antennas Propagat.*, vol. 39, pp.1024 -1030, 1991.

[4] J. Liu and Q. Xue, "Microstrip magnetic dipole Yagi array antenna with endfire radiation and vertical polarization," *IEEE Trans. Antennas Propag.*, vol. 61, no. 3, pp. 1140-1147, 2013.

[5] Z. Liang, J. Liu, Y. Zhang, and Y. Long, "A novel microstrip quasi Yagi array antenna with annular sector directors" *IEEE Trans. Antennas Propag.*, vol. 63, no. 10, pp.4524 -4529, Oct. 2015.

[6] M. Li, S. Q. Xiao, J. Xiong and B. Z. Wang, "Horizontal dipole located close to ground plane with bidirectional endfire radiation," *IEEE Antennas Wireless Propag. Lett.* , vol. 13, pp.1144 -1147, 2014.

[7] Z. Hu, Z. Shen, W. Wu and J. Lu, "Low-profile top-hat monopole antenna for end-fire radiation," *IEEE Trans. Antennas Propag.*, vol. 63, no. 7, pp.2851 -2857, Jul. 2015.

[8] L. Yang, J. Zhang, and W. Wu, "Wideband microstrip series-fed magnetic dipole array antenna," *IET Electron. Lett.*, vol. 50, no. 24, pp.1793 -1795, 2014.

[9] M. E. Morote, B. Fuchs, J.-F. Zürcher, and J. R. Mosig, "A printed transition for matching improvement of SIW horn antennas," *IEEE Trans. Antennas Propag.*, vol. 61, no. 4, pp. 1923–1930, Apr. 2013.

[10] M. E. Morote, B. Fuchs, J. F. Zurcher, and J. R. Mosig, "Novel thin and compact H-plane SIW horn antenna," *IEEE Trans. Antennas Propag.*, vol. 61, no. 6, pp. 2911–2920, Jun. 2013.

[11] S. Zhang, and G. F. Pedersen, "Netted waveguide antenna for UWB wind turbine blade deflection monitoring", *IEEE 5th Asia-Pacific Conference on Antennas and Propagation (APCAP)*, 2016.

[12] A. R. Mallahzadeh and S. Esfandiarpour, "Wideband H–plane horn antenna based on ridge substrate integrated waveguide (RSIW)," *IEEE Antennas Wireless Propag. Lett.*, vol. 11, pp. 85–88, Jan. 2012.

[13] Y. Zhao, Z. Shen, and W. Wu, "Wideband and low-profile H-plane ridged SIW horn antenna mounted on a large conducting plane," *IEEE Trans. Antennas Propag.*, vol. 62, no. 11, pp. 5895–5900, Nov. 2014.

[14] F. E. Butterfield, "Dielectric sheet radiators," *IRE Trans. Antennas Propag.*, vol. 2, no. 4, pp. 152–158, Oct. 1954.

[15] L. B. Felsen, "Radiation from a tapered surface wave antenna," *IRE Trans. Antennas Propag.*, vol. 8, no. 6, pp. 577–586, Nov. 1960.

[16] Z. Chen and Z. Shen, "Wideband flush-mounted surface wave antenna of very low profile," *IEEE Trans. Antennas Propag.*, vol. 63, no. 6, pp. 2430–2438, Jun. 2015.

[17] G. Kumar and K. C. Gupta, "Broadband microstrip antennas using additional resonators gap-coupled to the radiating edges," *IEEE Trans. Antennas Propagat.*, vol. AP–32, pp. 1375–1379, Dec. 1984.

[18] C. Rowell and R. Murch, "A capacitively loaded PIFA for compact mobile telephone handsets," *IEEE Trans. Antennas Propagat.*, vol. 45, pp. 837-842, 1997.

[19] C. Y. Chiu, K. M. Shum, and C. H. Chan, "A tunable via-patch loaded PIFA with size reduction," *IEEE Trans. Antennas Propag.*, vol. 55, no. 1, pp. 65–71, Jan. 2007.

[20] S. Zhang, K. Zhao, Z. Ying, and S. He, "Investigation of diagonal antenna-chassis mode in mobile terminal LTE MIMO antennas for bandwidth enhancement," *IEEE Antennas Propag. Mag.*, vol. 57, no. 2, pp. 217-228, Aug. 2015.

[21] J.-S. Hong and M. Lancaster, Microstrip Filters for RF/Microwave Applications, 2001: Wiley.

[22] S. Bedair, "Characteristics of some asymmetrical coupled transmission lines", *IEEE Trans. Microw. Theory Tech.*, vol. 32, no. 1, pp.108 -110, 1984.

[23] H. A. Wheeler, "Transmission line properties of parallel strips separated by a dielectric sheet," *IEEE Trans. Microwave Theory Tech.*, vol.13, pp. 172-185, 1965.

[24] R. Feick, H. Carrasco, M. Olmos, and H. D. Hristov, "PIFA input bandwidth enhancement by changing feed plate silhouette", *IET Electron. Lett.*, vol. 40, no. 15, pp. 921-922, 2004.